

# Synthesis, characterization and performance evaluation of Ni/Al<sub>2</sub>O<sub>3</sub> catalysts for reforming of crude ethanol for hydrogen production

Abayomi J. Akande<sup>a,b</sup>, Raphael O. Idem<sup>a,\*</sup>, Ajay K. Dalai<sup>b</sup>

<sup>a</sup> *Process Systems Engineering Laboratory, Faculty of Engineering, University of Regina, Regina, Sask., Canada S4S 0A2*

<sup>b</sup> *Department of Chemical Engineering, University of Saskatchewan, Saskatoon, Sask., Canada S7N 5C5*

Received 22 December 2004; received in revised form 16 March 2005; accepted 18 March 2005

Available online 17 May 2005

## Abstract

The effects of catalyst synthesis method (i.e. precipitation (PT), coprecipitation (CP) and impregnation (IM)), Ni loading and reduction temperature on the characteristics and performance of Ni/Al<sub>2</sub>O<sub>3</sub> catalysts were evaluated for the reforming of crude ethanol for H<sub>2</sub> production. The results showed that in the calcined PT catalysts, no NiAl<sub>2</sub>O<sub>4</sub> species were observed whereas this was a major species in CP and IM catalysts. As a result, PT catalysts were more reducible than CP and IM catalysts. PT catalysts exhibited slightly lower crystallite sizes of NiO species than the corresponding CP catalysts. On the other hand, IM catalysts had extremely large crystallite sizes except IM10 (IM catalyst with 10% Ni loading) which had the smallest crystallite size. A combination of small crystallite size and high reducibility for PT catalysts resulted in higher crude ethanol conversions for the PT catalysts. In contrast, the IM catalysts with larger crystallite sizes and lower reducibility yielded the lowest crude ethanol conversions. Catalysts with 15% Ni loading gave the best crude ethanol conversions for each method of synthesis with PT15 giving the best overall crude ethanol conversion of 85 mol% again because of its smaller crystallite size and higher reducibility. In terms of H<sub>2</sub> yield, CP15 was the optimum catalyst because of its higher H<sub>2</sub> selectivity as compared to PT15 and IM15 catalysts. Coking was observed at the onset of the reaction but stabilized after 180 min TOS.

© 2005 Elsevier B.V. All rights reserved.

**Keywords:** Ni–Al<sub>2</sub>O<sub>3</sub> catalysts; Synthesis method; Reducibility; Crude ethanol reforming; Crystallite size; Conversion

## 1. Introduction

The majority of current energy needs are supplied by combustion of non-renewable energy sources such as fossil fuels with the attendant release of large quantities of greenhouse gases (GHG), especially carbon dioxide (CO<sub>2</sub>) and other harmful emissions to the atmosphere. The gradual depletion of these fossil fuels reserves and efforts to combat pollution and greenhouse gas emissions have generated a considerable interest in using alternative sources of energy [1,2].

On the other hand, strong efforts are being made to commercialize the use of fuel cells such as the proton exchange membrane (PEM) fuel cell for the generation of electric power for both electric vehicles and distributed

electric power plants [3,4]. The major reason for the interest is the high energy efficiency of the fuel cell with an overall energy efficiency of about 60%, in some cases [5]. Also, with an equally strong interest in the use of hydrogen (H<sub>2</sub>) as the fuel, PEM fuel cells are the most certain to meet future ultra low NO<sub>x</sub>, SO<sub>x</sub>, CO, CH<sub>4</sub> and CO<sub>2</sub> emissions targets [3]. Thus, H<sub>2</sub> has a significant future potential as an alternative fuel that can solve the problems of CO<sub>2</sub> emissions as well as the emissions of other air contaminants. It is well known that H<sub>2</sub> production can be accomplished by gasification or reforming of fossil fuels [6,7] or biomass [8]. However, if a global cycle of clean and sustainable production of energy is envisaged, a new eco-friendly reservoir of hydrogen is needed. In this context, ethanol (a form of biomass) satisfies most of these requirements since it is easy to produce, and is also safe to handle, transport and store [9,10]. As such, ethanol provides an environmentally responsible energy source that can significantly reduce GHG emissions [2]. It is

\* Corresponding author. Tel.: +1 306 585 4470; fax: +1 306 585 4855.  
E-mail address: [raphael.idem@uregina.ca](mailto:raphael.idem@uregina.ca) (R.O. Idem).

also known that the application of ethanol for the production and use of H<sub>2</sub> energy is CO<sub>2</sub> neutral [11] as this does not result into any net emission of CO<sub>2</sub>. Furthermore, since ethanol does not contain heteroatoms and metals, its use as source of energy does not result in emissions of NO<sub>x</sub>, SO<sub>x</sub>, particulates and other toxics. In addition, ethanol is mostly an oxygenated hydrocarbon, which leads to complete combustion during its application to produce power. As such, little or no CO is produced. These attributes have made H<sub>2</sub> obtained from ethanol reforming a very good energy vector, especially in fuel cells applications. H<sub>2</sub> production from ethanol has advantages when compared with other H<sub>2</sub> production techniques, including steam reforming of methanol and hydrocarbons. Unlike hydrocarbons, ethanol is easier to reform and is also free of sulfur, which is a catalyst poison in the reforming of hydrocarbons [9]. Also, unlike methanol, which is sourced from hydrocarbons [12] and has a relatively high toxicity, ethanol is completely biomass based and has low toxicity.

The production of hydrogen by steam reforming of pure ethanol has been widely investigated. Jordi et al. [13] performed their investigation on Co/ZnO catalyst using a water to ethanol molar ratio of 13:1 (20%, v/v, ethanol) whereas Leclerc et al. [14] reported that water to ethanol ratios in the range of 20:1 (14%, v/v, ethanol) to 30:1 (10%, v/v, ethanol) enhanced hydrogen selectivity and inhibited the production of undesirable products such as methane (CH<sub>4</sub>), carbon monoxide (CO), acetaldehyde, ethylene and carbon. Gavita et al. [15] used water to ethanol molar ratios of 3:1 and 8.1:1, and obtained their highest ethanol conversion on Ni/MgO catalyst at water to ethanol molar ratio of 8.1:1 (28%, v/v, ethanol). Das [16] used a water to ethanol molar ratio of 6:1 (35%, v/v, ethanol) on Mn promoted Cu based catalyst to obtain optimum ethanol conversion, hydrogen yield and selectivity.

In all these cases, water is needed as a co-feed to the process. Consequently, there is no need to reduce the water and organic contents of wet or crude ethanol (fermentation broth produced from a fermentation process) since this contains approximately 12% (v/v) ethanol, which is within the range of water to ethanol molar ratio used for literature cited ethanol reforming processes. The reforming of crude ethanol is different from the reforming of pure ethanol essentially because of the presence of other oxygenated hydrocarbons such as glycerol, lactic acid and maltose. These have not been reported before to be steam reformed to produce hydrogen. In the first place, these oxygenated hydrocarbons add to an increased production of hydrogen by about 7% compared to steam reforming of pure ethanol. In the second place, the catalyst activity for ethanol reforming is influenced by the presence of the oxygenated hydrocarbons. Thirdly, the reaction temperature needs to be modified in order to accommodate the reforming of the oxygenated hydrocarbons. Also, this process would eliminate the large amount of energy wasted during distillation to remove water from fermentation broth in order to produce dry or pure ethanol. Haga et al. [2]

suggested that in order to obtain a widespread use of ethanol for hydrogen production, the economics and energetics of the ethanol production process have to be greatly improved. Thus, by circumventing the distillation and drying step, our process [17] of reforming crude ethanol (i.e. fermentation broth) provides us with the ability to produce H<sub>2</sub> from crude ethanol solution in a cost-effective manner. However, the reforming of crude ethanol to produce hydrogen has not been reported in the literature before, to the best of our knowledge, until we recently developed the catalytic process for H<sub>2</sub> production from the reforming of crude ethanol based on Cu/Mn/Al<sub>2</sub>O<sub>3</sub> and Ni/Al<sub>2</sub>O<sub>3</sub> catalysts [17].

Because of weight and engineering problems, on-board reforming to produce H<sub>2</sub> no longer appears to be the most attractive way to deliver H<sub>2</sub> to the fuel cell in electric vehicle. Instead, there are strong efforts to deliver the H<sub>2</sub> to the fuel cell for this application by means of H<sub>2</sub> refueling stations. Several such stations already exist, for example, Hydrogenics station in Toronto, Canada as well as stations in Perth, Australia and in Japan [18]. Also, a very important aspect for the actualization of the PEM fuel cell powered electric vehicles that would use crude ethanol based H<sub>2</sub> is the development of a stable active catalyst for the process. Such a catalyst should ensure high selectivity and yield and should result in a small sized reformer for use in a H<sub>2</sub> refueling station. While there is little information on catalysts development regarding the steam reforming of pure ethanol, there is no such information in the case of the reforming of crude ethanol. In the literature, Al<sub>2</sub>O<sub>3</sub> supported Co, Ni or Cu catalysts have been employed for pure ethanol reforming. Also, Idem et al. [17] indicated that Al<sub>2</sub>O<sub>3</sub> supported Ni catalysts or Cu–Mn–Al catalysts are active for crude ethanol reforming. Ni is reported [19] to ensure C–C bond breakage in ethanol or other oxygenated hydrocarbons while Al<sub>2</sub>O<sub>3</sub> ensures good thermal stability. Even though Ni/Al<sub>2</sub>O<sub>3</sub> catalysts appear to be the more active, the effects of the catalyst synthesis method, Ni loading and reduction temperature on the characteristics and performance of the catalysts have not been reported before for the reforming of crude ethanol for H<sub>2</sub> production. The evaluation of these effects are presented and discussed in this paper.

## 2. Experimental

Ni/Al<sub>2</sub>O<sub>3</sub> catalyst was selected based on the fact that Ni enhances steam-reforming reaction [15,17]. Also, it has been reported that Ni ensures C–C bond rupture of ethanol or other oxygenated hydrocarbon components of crude ethanol [17,19]. On the other hand, Al<sub>2</sub>O<sub>3</sub> was chosen as support because it ensures thermal stability of the catalyst [19,20].

### 2.1. Synthesis of catalysts

Three methods of synthesis: coprecipitation, precipitation and impregnation were investigated. The preparation

procedure used for coprecipitation was similar to the one used by Idem [21]. Briefly, the solution mixture of nickel nitrate hexahydrate and aluminum nitrate nonahydrate of appropriate concentration (depending on nickel loading) was prepared. Precipitation was brought about by adding this solution in a drop-wise manner with constant stirring to the solution of sodium carbonate solution ( $\text{pH} \cong 11.5$ ) maintained at  $40^\circ\text{C}$  in a 3-l flask. The quantity of sodium carbonate solution used was 1.1 times the stoichiometric requirement. The resulting slurry ( $\text{pH} \cong 8.0$ ) was vigorously stirred for another 60 min. The precipitate was filtered and dried at  $80^\circ\text{C}$  overnight. The dried precipitate was then washed several times with warm water and finally with cold water and then dried at  $110^\circ\text{C}$  overnight in air. The dried sample was then calcined, characterized and used for performance evaluation for the reforming of crude ethanol.

The precipitation synthesis method involved the preparation of solutions of predetermined amounts of nickel nitrate hexahydrate (depending on the Ni loading). This solution was added to another solution containing an appropriate quantity of sodium carbonate (to induce complete precipitation of the former), and which also contained commercial alumina. The commercial alumina was  $\gamma$ -alumina obtained from EM Science, Gibbstown, NJ, USA. The resulting slurry was vigorously stirred for 24 h to enhance precipitation of nickel on the  $\gamma$ -alumina. The precipitate was filtered and dried at  $80^\circ\text{C}$  overnight. The dried precipitate was then washed several times with warm water and finally with cold water and then dried at  $110^\circ\text{C}$  overnight in air. The dried sample was then calcined, characterized and used for performance evaluation for the reforming of crude ethanol.

The impregnation method involved preparation of nickel solutions of different concentrations dissolved in a solution of a fixed amount of the same type of commercial alumina ( $\gamma$ -alumina obtained from EM Science, Gibbstown, NJ, USA) as used in the precipitation method. The resulting slurry was stirred vigorously for 24 h and then filtered; the filtered sample was dried at  $110^\circ\text{C}$  overnight in air. The dried sample was analyzed for elemental composition by inductively coupled plasma-mass spectroscopy (ICP-MS). The information obtained was used to prepare a calibration

curve that was used for preparing catalysts with the desired Ni loading.

The designations and elemental compositions of the calcined catalysts are given in Table 1. CP, PT and IM indicate coprecipitation, precipitation and impregnation synthesis methods, respectively. The numbers in the designations in Table 1 represent the loadings while the symbols represent the synthesis method. For example, CP10 indicates a catalyst with 10% Ni loading prepared by coprecipitation synthesis method.

## 2.2. Catalyst characterization

The dried, calcined and reduced catalysts were characterized for BET surface area, pore size and distribution, and pore volume. The other characterization techniques to which these catalysts were subjected were temperature programmed reduction studies using  $\text{H}_2$  (TPR- $\text{H}_2$ ), thermogravimetric analysis (TGA), powder X-ray diffraction (XRD) analysis, X-ray line broadening, and temperature programmed oxidation (TPO). BET surface area, pore volume and pore size distribution of the catalysts were measured by  $\text{N}_2$  adsorption at 77 K using a Micromeritics adsorption equipment (Model ASAP 2010, manufactured by Micromeritics Instruments Inc., Norcross, GA, USA) using  $\text{N}_2$  gas (99.995% pure; obtained from Praxair, Regina, Saskatchewan, Canada). TPR- $\text{H}_2$  studies were performed with ChemBET3000, manufactured by Quantachrome Corporation, FL, USA. This equipment was fitted with a thermal conductivity detector (TCD), and analysis was done using 5 mol%  $\text{H}_2$  in  $\text{N}_2$  at a heating rate of  $10^\circ\text{C}/\text{min}$  from room temperature to  $900^\circ\text{C}$ . TGA was performed to measure the weight loss, the rate of weight loss and the heat effects associated with drying, combustion or decomposition of catalyst as a function of temperature. The analysis was performed with TG-DSC-1100 supplied by Setaram Scientific and Industrial Equipment, NJ, USA. At different stages of synthesis, the powder XRD patterns of all the catalysts were obtained with D8 diffractometer with GADDS equipped with a Cu source both manufactured by Bruker AXS, USA, in order to identify the component phases present as a function of synthesis method. This

Table 1  
Name and chemical composition of catalysts

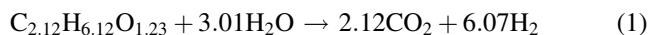
Preparation method	Catalyst name	Ni composition (wt.%)	Al composition (wt.%)	O composition (wt.%)
Coprecipitation	CP10	10	47.63	42.37
	CP15	15	44.98	40.02
	CP20	20	42.34	37.66
	CP25	25	39.69	35.31
Precipitation	PT10	10	47.63	42.37
	PT15	15	44.98	40.02
	PT20	20	42.34	37.66
Impregnation	IM10	10	47.63	42.37
	IM15	15	44.98	40.02
	IM20	20	42.34	37.66

applied to dried, calcined and reduced catalyst samples. The X-ray diffractograms were recorded at  $2\theta$  angles ranging from  $4^\circ$  to  $100^\circ$  at a speed of  $5^\circ/\text{min}$ . The crystallite sizes of the samples were also obtained by X-ray line broadening using the same equipment. After the crude ethanol reforming reaction, the catalysts were characterized by means of TPO under an oxidative atmosphere (5% oxygen in helium) flowing at 30 mL/min at a temperature-programmed rate of  $10^\circ\text{C}/\text{min}$  using the Perkin Elmer Pyris Diamond TG/DTA supplied by Seiko Instruments Inc., USA.

### 2.3. Catalytic activity tests

#### 2.3.1. The feed material

The feed for this process was crude ethanol (i.e. fermentation broth) and was obtained from Pound Maker Adventures, Lanigan, Saskatchewan, Canada. This was used as received except for the removal of particulate matter by filtration. However, for the purpose of evaluating the performance of the catalysts, crude ethanol was defined as the combination of all the oxygenated hydrocarbon components present in fermentation broth; namely, ethanol, lactic acid, glycerol and maltose. We performed an analysis in our laboratory to both identify and quantify these components of fermentation broth using a high performance liquid chromatograph (HPLC) Model Agilent 1100 series supplied by Agilent Technologies, Wilmington, DE, USA. The HPLC was equipped with a  $250\text{ mm} \times 4.1\text{ mm}$  HC-75 column and a refractive index detector, while 0.05 mM succinic acid was used as the mobile phase. The result of the analysis is shown in Table 2. Consequently, the overall molecular formula of crude ethanol based on the weighted average of these components is  $\text{C}_{2.12}\text{H}_{6.12}\text{O}_{1.23}$ . Based on this composition, the general equation representing the reforming of crude ethanol can be represented as in Eq. (1).



#### 2.3.2. Activity tests

The reactor used to obtain experimental data was BTRS model number 02250192-1 supplied by Autoclave Engineers, Erie, PA, USA. It was made of a stainless steel tube of 8.0 mm internal diameter ( $D$ ) placed in an electric furnace. Crude ethanol was delivered to the reactor chamber by means of a HPLC pump regulated at the desired flow rates. The reaction temperature was measured with a sliding

thermocouple placed inside the bed. The error on temperature measurement was within  $\pm 1^\circ\text{C}$ .

A typical run for the reforming of crude ethanol was performed as follows: approximately 1 g of the catalyst was mixed with 2 g of Pyrex glass (i.e. inert material) of the same average particle size and then loaded into the reactor. The feed consisting of crude ethanol (comprising of ethanol plus other organics and water) was then pumped at the desired flow rate (i.e. space velocity) to the vaporizer maintained at  $250^\circ\text{C}$  before entering the reactor. Prior to reaction the catalyst was reduced in situ by treatment with 5%  $\text{H}_2$  in  $\text{N}_2$  gas (supplied by Praxair, Regina, Saskatchewan, Canada) flowing at 100 mL/min for 2 h. The reactions were carried out at atmospheric pressure and reaction temperature of  $400^\circ\text{C}$ . The product mixture during reaction was passed through a condenser and gas–liquid separator to separate the gaseous and liquid products for analysis.

#### 2.3.3. Analysis of liquid and gaseous products

The liquid product was analyzed using the same HPLC described earlier. This liquid product was also analyzed with GC–MS in order to identify the components for subsequent HPLC analysis. GC–MS analysis was performed using GC–MS model HP 6890/5073 supplied by Hewlett-Packard, Quebec, Canada. An HP–Innowax column (length = 30 m, internal diameter =  $250\ \mu\text{m}$ , thickness =  $0.25\ \mu\text{m}$ ) packed with cross-linked poly-ethylene glycol was used in the GC for the separation of components. The composition of the output gas stream was analyzed on-line by gas chromatography (Model HP 6890) using molecular sieve and Haysep columns, a thermal conductivity detector (TCD) and helium as carrier gas. The schematic diagram of the experimental set-up used for the reforming reaction is shown in Fig. 1.

## 3. Results and discussion

### 3.1. Catalyst characteristics

#### 3.1.1. BET surface area, pore size and pore volume

BET surface area, pore volume and pore size studies were performed on the calcined catalysts. The results are given in Table 3 for pore volume and average pore size and in Fig. 2 for BET surface area. In the coprecipitation method, the BET surface area (Fig. 2) decreased in a monotonic fashion from 83 to  $65\ \text{m}^2/\text{g}$  as the Ni loading increased. In contrast, the pore size and pore volume initially increased with Ni loading and reached a maximum of 14.5 nm and  $0.29\ \text{cm}^3/\text{g}$ , respectively, and then decreased with further increase in the Ni loading. Calcined catalysts prepared by precipitation and impregnation methods exhibited similar trends in surface area and pore size as those prepared by the coprecipitation method. However, the pore sizes of the CP catalysts were much larger than the corresponding PT and IM catalysts. On the other hand, the pore volume for which the catalysts were

Table 2  
Crude ethanol composition

Crude ethanol components	vol.%	mol% on a water free basis
Ethanol	12	88.42
Lactic acid	1	5.71
Glycerol	1	5.87
Maltose	0.001	0.001
Water	86	Not applicable

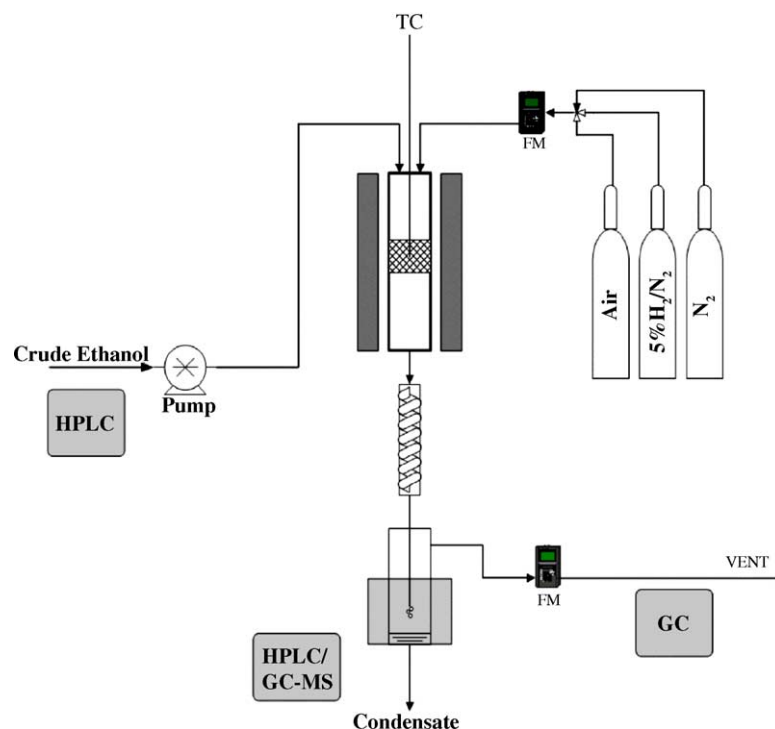


Fig. 1. Schematic diagram of the experimental rig for the production of hydrogen by the reforming of crude ethanol.

synthesized by precipitation and impregnation methods showed a somewhat different trend as compared to the trend for precipitation. It was observed in the PT and IM catalysts that 10% and 15% Ni loading catalysts gave identical values in each case.

### 3.1.2. Powder X-ray diffraction (XRD)

Powder XRD analyses were performed on the dried, calcined and reduced catalysts to identify the species present in the catalysts at various stages of synthesis. Fig. 3 shows the XRD spectra obtained for dried (Fig. 3a), calcined (Fig. 3b–d) and reduced (Fig. 3e) catalysts. Typical spectra of dried catalysts (15% Ni loading) exhibited common XRD peaks corresponding to nickel hydroxide ( $\text{Ni}(\text{OH})_2 \cdot 4\text{H}_2\text{O}$ ) and nickel oxide hydroxide ( $\text{NiOOH}$ ). Only the catalyst prepared by the impregnation method gave XRD peaks corresponding to hydrated alumina ( $\text{Al}_2\text{O}_3 \cdot 3\text{H}_2\text{O}$ ) whereas

the catalyst prepared by coprecipitation had XRD peaks corresponding to nickel aluminum carbonate hydroxide ( $\text{Ni}_2\text{Al}(\text{CO}_3)_2(\text{OH})_3$  and  $\text{NiAl}(\text{CO}_3)(\text{OH})_3$ ) as well as nickel carbonate hydroxide hydrate ( $\text{Ni}_2(\text{CO}_3)(\text{OH})_2 \cdot 4\text{H}_2\text{O}$ ). The catalysts prepared by the coprecipitation and precipitation methods exhibited XRD peaks corresponding to aluminum carbonate hydroxide ( $\text{Al}(\text{CO}_3)_2(\text{OH})_4 \cdot 3\text{H}_2\text{O}$  and  $\text{Al}(\text{CO}_3)(\text{OH})$ ). The formation of nickel aluminum carbonate hydroxide, nickel carbonate hydroxide hydrate and aluminum carbonate hydroxide were attributed to using  $\text{Na}_2\text{CO}_3$  for precipitation [21].

Table 3  
Pore volume and pore sizes of catalysts

Catalyst name	Pore volume ( $\text{cm}^3/\text{g}$ )	Pore diameter (nm)
CP10	0.26	12.6
CP15	0.29	14.5
CP20	0.22	12.8
CP25	0.19	12.0
PT10	0.23	5.4
PT15	0.22	5.6
PT20	0.12	5.4
IM10	0.18	4.3
IM15	0.18	4.6
IM20	0.17	4.5

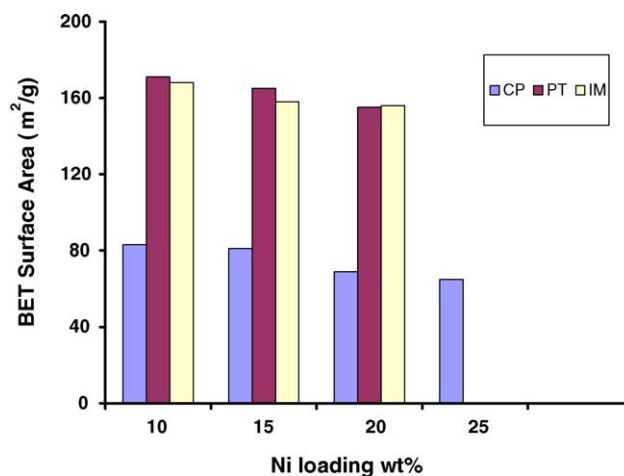


Fig. 2. BET surface areas as function of Ni loading for catalysts calcined at 600 °C.

Catalysts prepared by all the three different methods were compared at different Ni loadings in the case of calcined catalysts. For the catalysts with 10% Ni loading, the XRD spectra (Fig. 3b) showed common peaks corresponding to nickel oxide (NiO), alumina ( $\text{Al}_2\text{O}_3$ ) and nickel aluminate ( $\text{NiAl}_2\text{O}_4$ ) even though the latter was only pronounced for IM10 whereas for the catalysts with 15% Ni loading, only nickel oxide and alumina were the common species. Nickel aluminate was observed only on coprecipitated (CP15) and impregnated (IM15) samples. The same scenario was observed for the catalyst samples with 20% Ni loading. The formation of nickel aluminate was attributed to the close interaction between NiO and  $\text{Al}_2\text{O}_3$  at a high temperature as shown in Eq. (2) mainly for impregnated catalyst samples or

the decomposition of nickel aluminum carbonate hydroxide followed by Eq. (2) for coprecipitated catalyst samples.



The formation of nickel aluminate is an indication of strong metal–support interaction. Also, the appearance of peaks corresponding to nickel species is an indication of strong crystallinity of the species and that monolayer coverage of  $\text{Al}_2\text{O}_3$  by the applicable Ni species was exceeded. On the other hand, the absence of some of the Ni species (such as  $\text{NiAl}_2\text{O}_4$ ) in some of the calcined catalyst samples (e.g. the PT catalysts) is an indication that Ni species is still within monolayer coverage (i.e. the amount

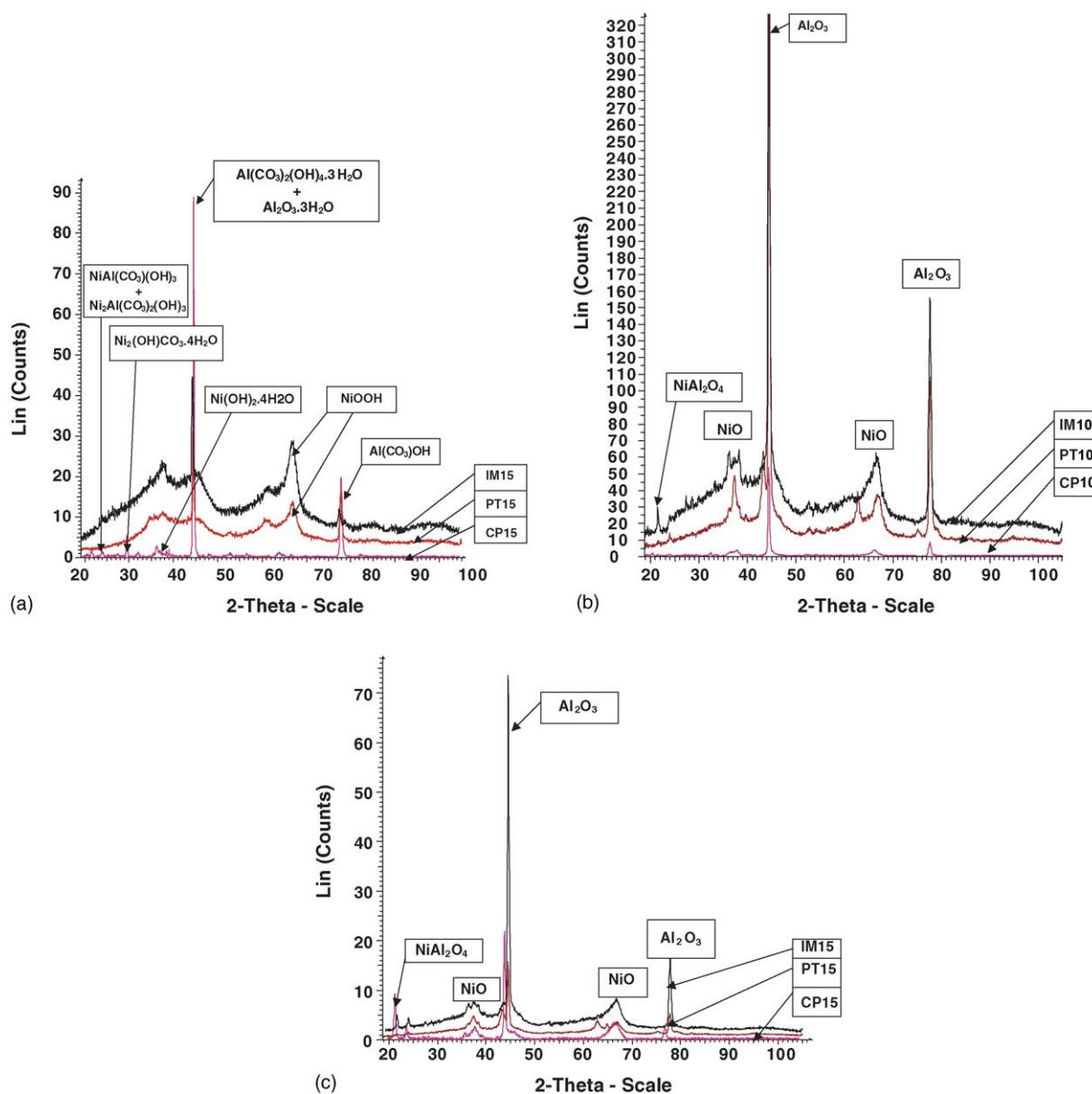


Fig. 3. XRD pattern of catalysts: (a) dried catalysts (15% Ni loading); (b) calcined catalysts (10% Ni loading); (c) calcined catalysts (15% Ni loading); (d) calcined catalysts (20% Ni loading); (e) reduced catalysts (15% Ni loading).

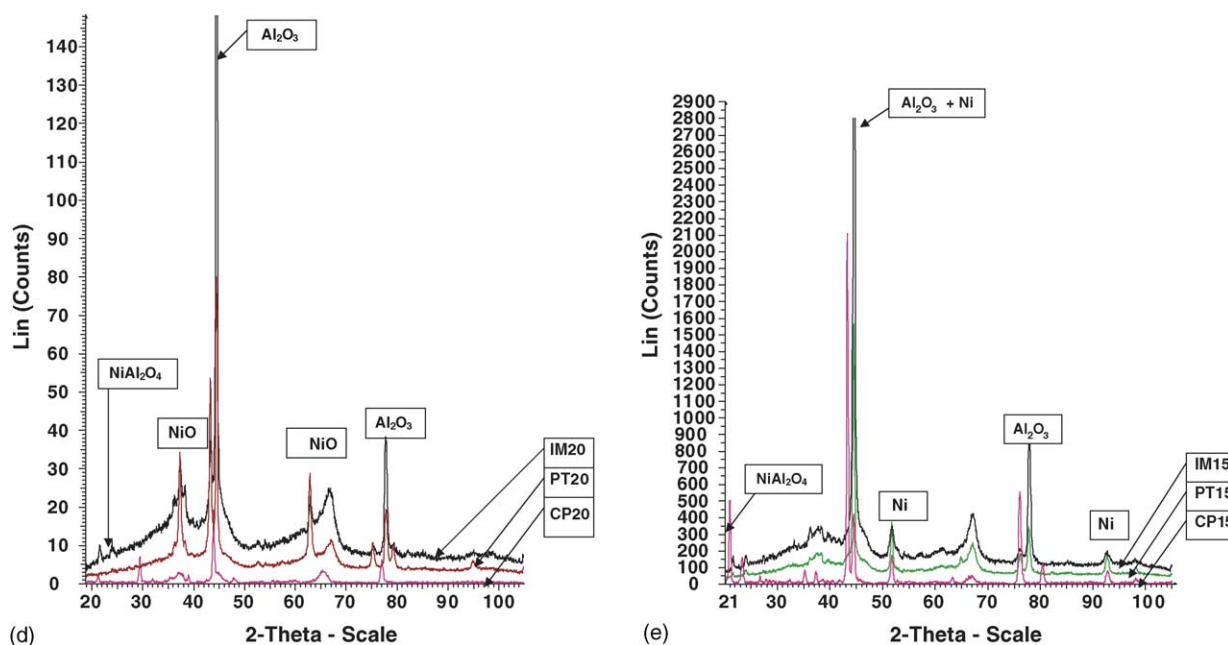


Fig. 3. (Continued).

present is too small and thus cannot be detected by XRD or is completely absent.

In the case of the reduced catalysts, typical XRD spectra for catalysts with 15% Ni loading (Fig. 3e) showed common peaks corresponding to nickel metal (Ni) and aluminum oxide. The spinel, nickel aluminate, was observed only for catalysts prepared by coprecipitation and impregnation methods. This shows that the reduction temperature of 600 °C used for catalyst reduction with  $\text{H}_2$  was not sufficient to reduce all the nickel aluminate species to Ni metal and alumina for these two types of catalysts.

Table 4 shows the results of crystallite size measurements for NiO species obtained by X-ray line broadening as a function of preparation method and Ni loading. At 10% Ni loading all catalysts have relatively small crystallite sizes with that prepared by impregnation having the smallest crystallite size. However, with Ni loadings of 15% and 20%, the catalysts prepared by the impregnation method produced a dramatic increase in crystallite size (105.8 and 160.2 nm, respectively). These were much larger than the crystallite sizes of the corresponding Ni loadings for catalysts prepared

Table 4  
Crystallite size of catalysts

Catalysts name	Crystallite size (nm)
CP10	26.5
CP15	29.8
CP20	38.5
PT10	21.5
PT15	20.8
PT20	39.6
IM10	15.3
IM15	105.8
IM20	160.2

by coprecipitation and precipitation methods. The overall large crystallite sizes (especially for Ni loading  $\geq 15\%$ ) shows the existence of agglomeration of Ni species and that monolayer coverage was exceeded.

### 3.1.3. Thermogravimetric analysis

The evaluation of weight loss, rate of weight loss as well as the heat effects associated with drying or decomposition of dried catalysts as a function of temperature is important because it enables us to determine the maximum temperature after which the catalyst weight loss is negligible (i.e. complete decomposition). This, in turn, allows us to establish the minimum temperature at which catalyst becomes thermally stable, and as such, the minimum temperature for catalyst calcination.

The TGA profiles for dried catalysts samples are shown in Fig. 4a–i. The profiles of these dried catalysts, in general, show an endothermic peak at about 100 °C corresponding to thermal desorption of  $\text{H}_2\text{O}$  and adsorbed  $\text{CO}_2$  as reported by Jianjun et al. [22]. The peak at about 250–350 °C corresponds to the abstraction of chemically bound water from nickel hydroxide hydrate ( $\text{Ni}(\text{OH})_2 \cdot 4\text{H}_2\text{O}$ ) and aluminum hydroxide. It could also correspond to the thermal decomposition of nickel aluminum carbonate hydroxide ( $\text{Ni}_2\text{Al}(\text{CO}_3)_2(\text{OH})_3$ ) by removal of  $\text{CO}_2$ . The endothermic peak at about 500–600 °C corresponds to the thermal decomposition of nickel hydroxide into NiO and  $\text{H}_2\text{O}$  as reported by Parthasarathi et al. [23] and the thermal decomposition of nickel aluminum hydroxide into  $\text{NiAl}_2\text{O}_4$  and  $\text{H}_2\text{O}$ . The nickel hydroxide described in the former case results from the elimination of  $\text{H}_2\text{O}$  and  $\text{CO}_2$  from  $\text{Ni}_2(\text{OH})\text{CO}_3 \cdot 4\text{H}_2\text{O}$  and by abstraction of  $\text{H}_2\text{O}$  from  $\text{Ni}(\text{OH})_2 \cdot 4\text{H}_2\text{O}$ . Since the peak that was observed specifi-

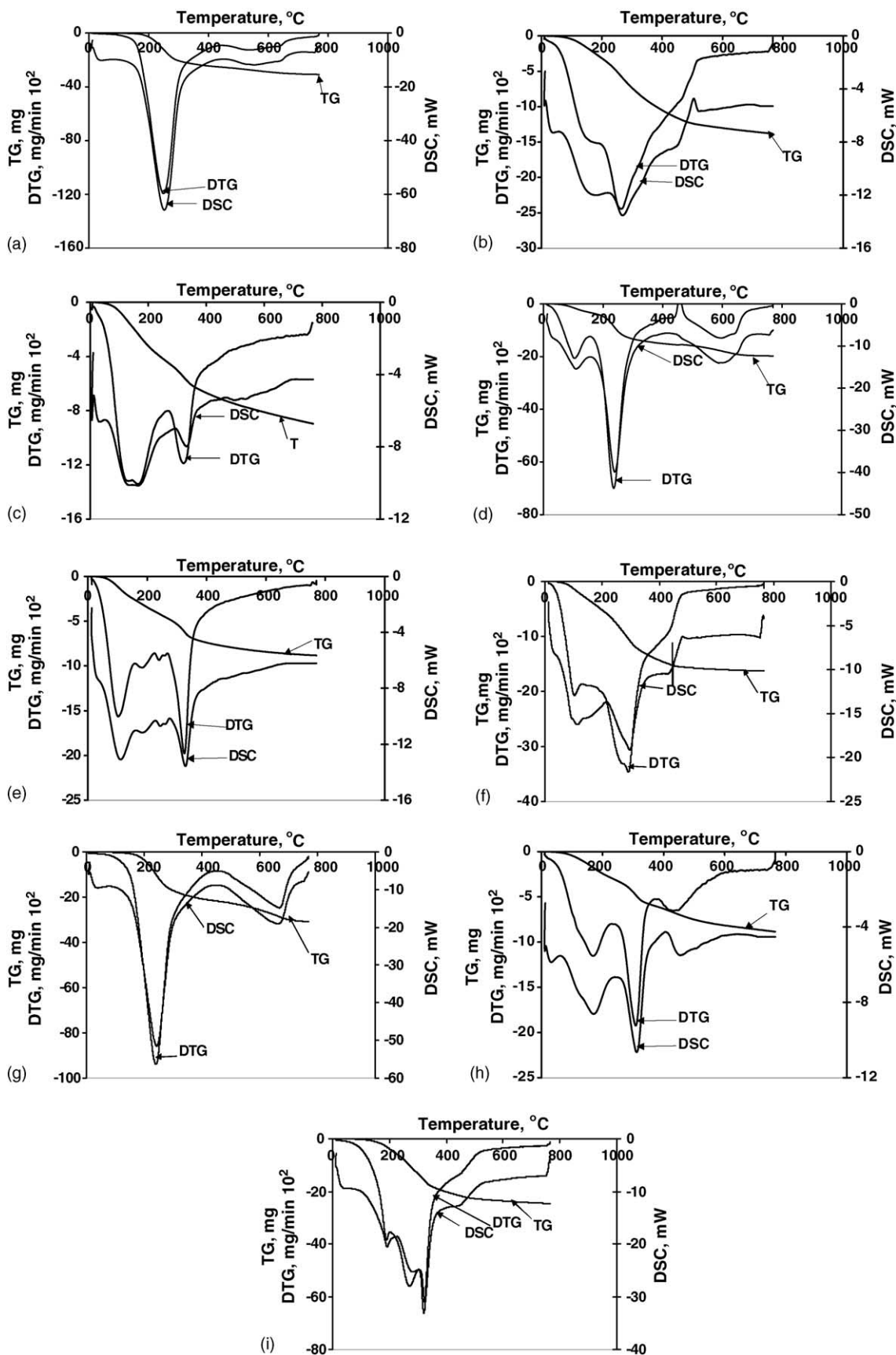


Fig. 4. TG-DSC profile of CP10 catalyst: (a) dried CP10 catalyst; (b) dried PT10 catalyst; (c) dried IM10 catalyst; (d) dried CP15 catalyst; (e) dried PT15 catalyst; (f) dried IM15 catalyst; (g) dried CP20 catalyst; (h) dried PT20 catalyst; (i) dried IM20 catalyst.

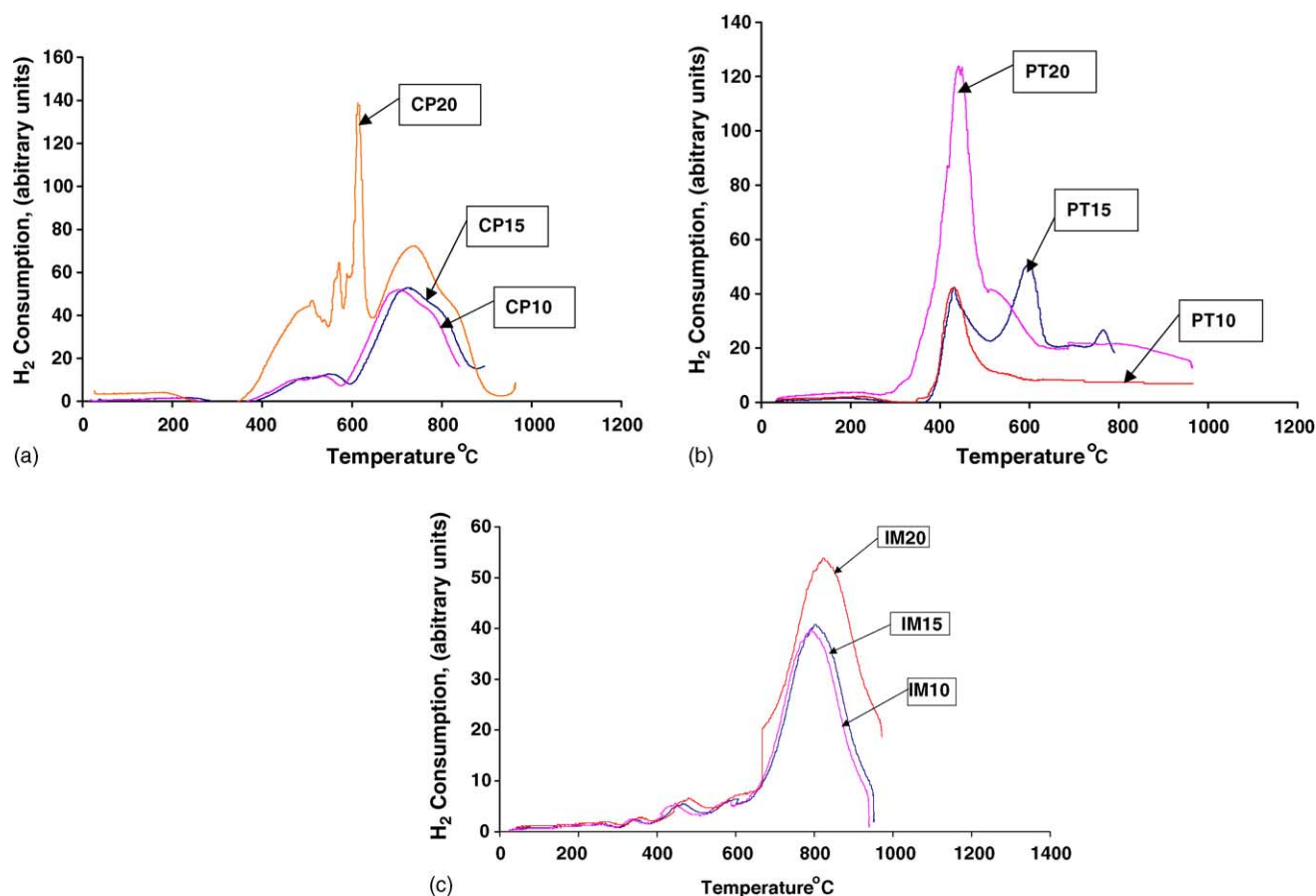


Fig. 5. TPR-H<sub>2</sub> profiles of calcined catalysts prepared by: (a) the coprecipitation method; (b) the precipitation method; (c) the impregnation method.

cally at 600 °C was obtained only in the CP catalysts and was absent in the PT and IM catalysts, it can be concluded that the Ni(OH)<sub>2</sub> in this case originated from Ni<sub>2</sub>(OH)CO<sub>3</sub>·4H<sub>2</sub>O whereas the one at about 500 °C originated from Ni(OH)<sub>2</sub>·4H<sub>2</sub>O. Also, since the peak at 600 °C is specific to the CP catalysts, the results imply that the decomposition of nickel aluminum hydroxide to yield NiAl<sub>2</sub>O<sub>4</sub> occurs at this temperature. The TG profiles for these dried catalyst samples suggest that the calcination temperature of 600 °C was adequate and was able to stabilize all the catalysts except in CP20 where a calcinations temperature of 650 °C would be required for stabilizing the catalyst.

#### 3.1.4. Temperature programmed reduction (TPR-H<sub>2</sub>)

The objective of TPR-H<sub>2</sub> experiments was to determine the reducibility as well as the optimum reduction temperature for the catalysts for the reforming of crude ethanol. In conjunction with XRD data, it was also useful in determining the type of species present in the calcined catalysts. The TPR-H<sub>2</sub> profiles of all the catalysts calcined at 600 °C are given in Fig. 5a–c for catalysts prepared by coprecipitation, precipitation and impregnation, respectively. The peak temperatures and the corresponding species are summarized in Table 5.

All the reduction peaks between 400 and 602 °C represent the reduction of NiO. The oxide of nickel was produced by the thermal decomposition of various non-aluminum containing nickel species at appropriate temperatures, as evidenced from XRD and TGA studies. The presence of these peaks has been reported by Idem et al. [24] for Co–Ni–ZrO<sub>2</sub>/sulphated-ZrO<sub>2</sub> hybrid catalysts and by Jae-Hee et al. [25] for Ni/Al<sub>2</sub>O<sub>3</sub> catalyst. The peaks observed in the temperature range of 750–812 °C represent the reduction of NiAl<sub>2</sub>O<sub>4</sub> species. The presence of this peak has been reported by Marino et al. [26], Jae-Hee et al. [25] and

Table 5  
Summary of TPR analyses for calcined Ni/Al<sub>2</sub>O<sub>3</sub> catalysts

Catalysts name	Number of peaks	Peak temperature (°C)	Major reducible species
CP10	3	471, 534, 700	NiO, NiAl <sub>2</sub> O <sub>4</sub>
CP15	3	501, 569, 731	NiO, NiAl <sub>2</sub> O <sub>4</sub>
CP20	3	514, 572, 738	NiO, NiAl <sub>2</sub> O <sub>4</sub>
PT10	2	438, 600	NiO
PT15	3	434, 602, 769	NiO
PT20	2	446, 529	NiO
IM10	3	444, 594, 794	NiO, NiAl <sub>2</sub> O <sub>4</sub>
IM15	3	472, 602, 812	NiO, NiAl <sub>2</sub> O <sub>4</sub>
IM20	3	488, 612, 830	NiO, NiAl <sub>2</sub> O <sub>3</sub>

Juan-Juan et al. [27] for Ni/Al<sub>2</sub>O<sub>3</sub> and Cu–Ni/Al<sub>2</sub>O<sub>3</sub> catalysts.

The reduction temperature and the peak width are indications of the ease of reduction and the degree of interaction between different species, respectively. High reduction temperature indicates difficulty in reduction whereas wide peaks indicate a great degree of interaction between the species and the support. It is seen from TPR-H<sub>2</sub> profile that the PT catalysts are almost completely reduced at 600 °C whereas the CP and IM catalysts require a higher reduction temperature (approximately 800 °C) due to the presence of the NiAl<sub>2</sub>O<sub>4</sub> species. This implies that PT catalysts have higher reducibility than the CP and IM catalysts. It is important to note that the respective major higher TPR-H<sub>2</sub> peak temperatures (about 800 °C) for the IM and CP catalysts increased with the Ni loading, implying that reducibility decreased with the Ni loading. In contrast, the major higher TPR-H<sub>2</sub> peak temperature (600 °C) in the case of PT catalysts shifted to lower temperatures as the Ni loading increased implying that reducibility increased with Ni loading. Also, the TPR-H<sub>2</sub> peaks for the PT catalysts were narrower than those for the CP and IM catalysts implying a higher degree of interaction of Ni species with Al<sub>2</sub>O<sub>3</sub> for CP and IM catalysts, as evidenced by the presence of NiAl<sub>2</sub>O<sub>4</sub>.

### 3.2. Catalyst performance evaluation

The catalysts were evaluated for their performance in the reforming of crude ethanol. The evaluation criteria used were crude ethanol conversion, H<sub>2</sub> selectivity and H<sub>2</sub> yield. Crude ethanol conversion was defined according to Eq. (3) while H<sub>2</sub> yield and selectivity were defined according to Eqs. (4) and (5), respectively.

Crude conversion ( $X$ )

$$= \frac{\text{gmol (organics) in} - \text{gmol (organics) out}}{\text{gmol (organics) in}} \quad (3)$$

where organics = ethanol + lactic acid + glycerol + maltose.

$$\text{Hydrogen yield (} Y \text{)} = \frac{\text{gmol (H}_2\text{) out}}{6.07 \times \text{gmol (organics) in}} \quad (4)$$

Hydrogen selectivity ( $S$ )

$$= \frac{\text{gmol (H}_2\text{) out}}{6.07 \times \text{gmol (organics) in} \times \text{conversion (} X \text{)}} \quad (5)$$

We have also used turnover number (TON) for crude ethanol conversion as one of the criteria for evaluating the activity of the catalysts. This is defined as ethanol conversion per mole of Ni in the catalyst as shown in Eq. (6).

Turnover number for crude ethanol conversion (TON)

$$= \frac{\text{crude ethanol conversion}}{\text{mol of Ni in catalysts}} \quad (6)$$

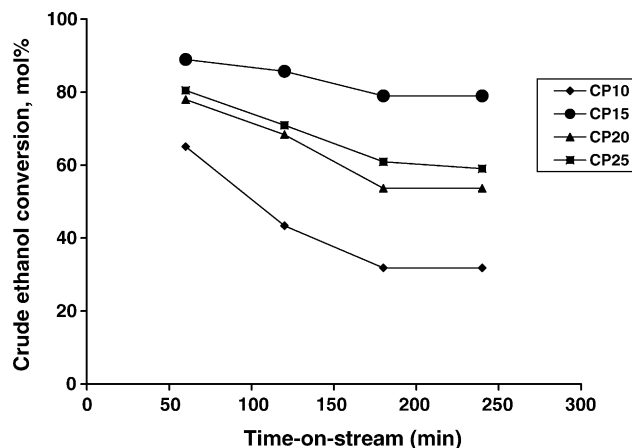


Fig. 6. Conversion of crude ethanol as a function of time-on-stream (TOS) on catalyst prepared by coprecipitation method at  $T = 400$  °C, WHSV =  $1.68 \text{ h}^{-1}$ , reduction temperature =  $600$  °C and calcination temperature =  $600$  °C.

#### 3.2.1. Crude ethanol conversion

This evaluation was carried out on all prepared catalysts at a weight hourly space velocity (WHSV) of crude ethanol (i.e. with respect to organics only) of  $1.68 \text{ h}^{-1}$  and reaction temperature of  $400$  °C. All catalysts were calcined at  $600$  °C for 3 h and reduced at  $600$  °C for 2 h. Fig. 6 shows the crude ethanol conversion behavior for catalysts prepared by the coprecipitation method. It is seen in the figure that each catalyst showed an initial high activity with a high initial crude ethanol conversion. This was attributed to the initial wild activity of the catalysts. The conversion decreased with time and then stabilized at about 180 min time-on-stream (TOS). CP15 gave the highest stable conversion of crude ethanol (79 mol%), followed by CP25 (59 mol%) while CP10 gave the lowest conversion (32 mol%) under the same experimental conditions. Fig. 7

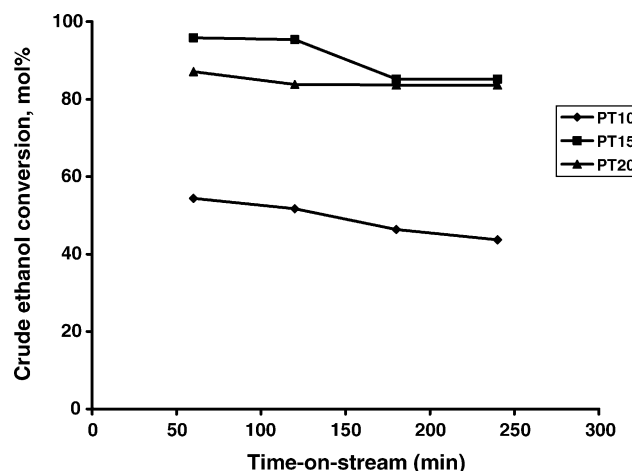


Fig. 7. Conversion of crude ethanol as a function of time-on-stream (TOS) on catalyst prepared by precipitation method at  $T = 400$  °C, WHSV =  $1.68 \text{ h}^{-1}$ , reduction temperature =  $600$  °C and calcination temperature =  $600$  °C.

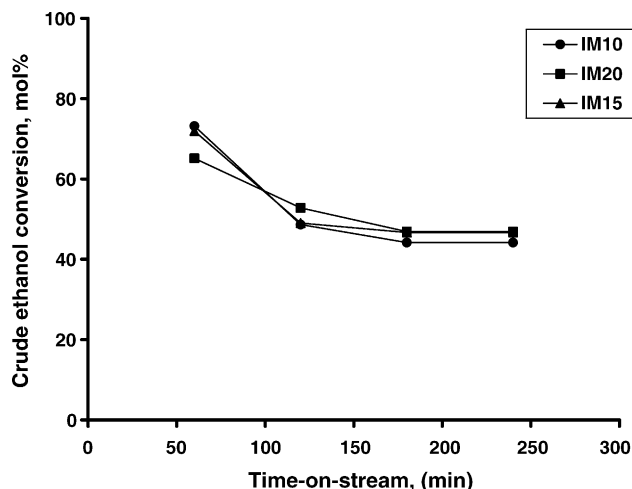


Fig. 8. Conversion of crude ethanol as a function time-on-stream (TOS) on catalyst prepared by impregnation method at  $T = 400\text{ }^{\circ}\text{C}$ ,  $\text{WHSV} = 1.68\text{ h}^{-1}$ , reduction temperature =  $600\text{ }^{\circ}\text{C}$  and calcination temperature =  $600\text{ }^{\circ}\text{C}$ .

gives crude ethanol conversions for the catalysts prepared by the precipitation method. The figure shows trends similar to those exhibited by catalysts prepared by the coprecipitated method. Similar reasons as for the trend in the coprecipitated method could also be used to explain the behavior. Also, the highest stable conversion of crude ethanol was obtained on PT15 (85 mol%). This was followed by PT20 (83 mol%) while the lowest conversion was obtained on PT10 (44.1 mol%). Fig. 8 shows that the trend for crude ethanol conversion as a function of time-on-stream obtained on catalysts prepared by the impregnation method were similar to those for the CP and PT catalysts. It was observed that the IM15 and IM20 did not show any significant difference in their crude ethanol conversion activities as stable crude ethanol conversions of 46.7 and 46.9 mol% were, respectively, obtained on these catalysts. On the other hand, IM10 gave a lower stable conversion of 44.2 mol%.

In order to evaluate the effect of Ni loading, we compared the stable crude ethanol conversions obtained on catalysts prepared by the three methods as a function of Ni loading. The results are given in Fig. 9. For catalysts prepared by coprecipitation, the stable conversion increased with Ni loading and reached a maximum value of 79 mol% at a Ni loading of 15 wt.%. Beyond this loading, the conversion of crude ethanol decreased. A similar trend was observed in the case of catalysts prepared by the precipitation method for which the lowest stable conversion was 44 mol% by PT10 and the maximum stable conversion was 85 mol% by PT15. Catalysts prepared by impregnation method exhibited a slightly different trend in which crude ethanol conversion reached a maximum value of 46.7 mol% on IM15 from 44 mol% on IM10. A further increase from 15% to 20% Ni loading did not result in any appreciable change in crude ethanol conversion.

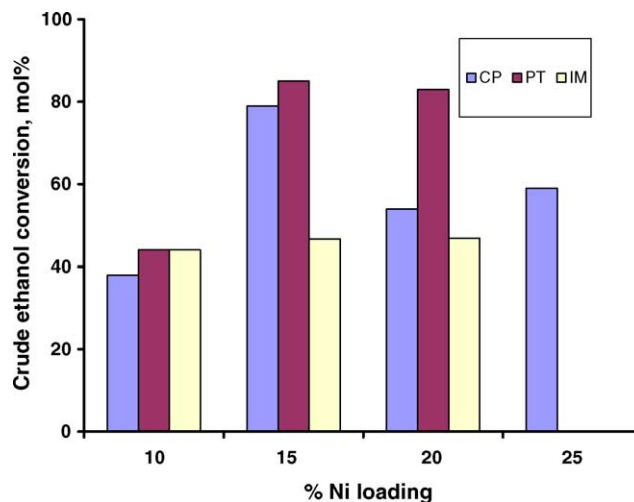


Fig. 9. Comparison of stable conversion of crude ethanol on various catalysts at  $T = 400\text{ }^{\circ}\text{C}$ , reduction temperature =  $600\text{ }^{\circ}\text{C}$ , calcination temperature =  $600\text{ }^{\circ}\text{C}$  and  $\text{WHSV} = 1.68\text{ h}^{-1}$ .

### 3.2.2. Turnover number (TON)

The results for TON as a function of nickel loading are given in Fig. 10. The figure shows that for catalyst prepared by coprecipitation, the TON increased with nickel loading from 10% to 15% and reached a maximum value of 309/mol of Ni, further increase in nickel loading led to a decrease in the TON. Similar results were obtained on catalysts prepared by precipitation, for which a maximum TON of 332/mol of Ni was obtained on PT15. The TON decreased thereafter as the nickel loading increased. Catalysts prepared by impregnation showed a different behaviour in which the TON decreased progressively with an increase in nickel loading from 10% to 20%.

### 3.2.3. Hydrogen yield

The activities of all the catalysts were also evaluated in terms of  $\text{H}_2$  yield as defined in Eq. (4). It is important to note

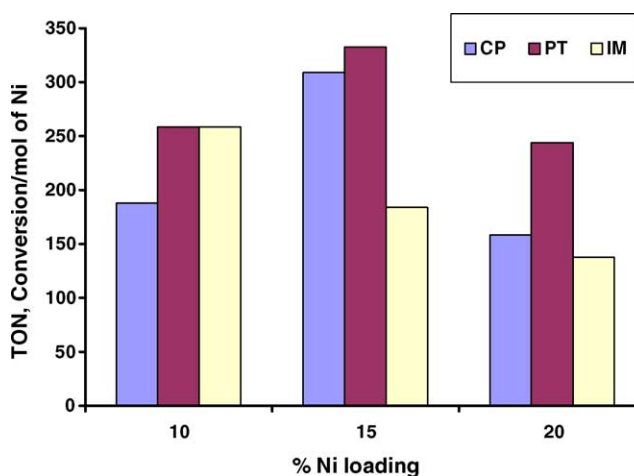


Fig. 10. Variation of turnover number (TON) with Ni loading at  $T = 400\text{ }^{\circ}\text{C}$ , reduction temperature =  $600\text{ }^{\circ}\text{C}$ , calcination temperature =  $600\text{ }^{\circ}\text{C}$  and  $\text{WHSV} = 1.68\text{ h}^{-1}$ .

that H<sub>2</sub> yields obtained were generally about 7% higher than what would be obtained from pure ethanol alone. The extra yield came from the conversion of the other oxygenated compounds (i.e. glycerol, lactic acid and maltose). Fig. 11 illustrates the variation of H<sub>2</sub> yield as a function of Ni loading. CP10 gave a H<sub>2</sub> yield of 2.12 mol H<sub>2</sub>/mol crude ethanol fed, the yield increased as Ni loading increased and reached a maximum of 4.33 mol H<sub>2</sub>/mol crude ethanol fed on CP15, and then decreased as the Ni loading increased beyond 15%. Similar trends were obtained in both the catalysts prepared by precipitation and impregnation methods with maximum H<sub>2</sub> yields of 4.24 and 2.52 mol H<sub>2</sub>/mol crude ethanol fed obtained on PT15 and IM15, respectively. Since the production of hydrogen was a major objective in this work, catalyst CP15 was considered the optimum catalyst. This is because it gave the highest hydrogen yield of 4.33 mol H<sub>2</sub>/mol crude ethanol fed, and also had a high stable crude ethanol conversion of 79 mol% even though slightly lower than that for PT15 (85 mol%).

### 3.2.4. Hydrogen selectivity

The higher H<sub>2</sub> yield for CP15 as compared with PT15 (that gave a higher crude ethanol conversion) was attributed to the higher H<sub>2</sub> selectivity of CP15. This was confirmed in Fig. 12, which shows the variation of H<sub>2</sub> selectivity with Ni loading for all catalysts. Catalysts prepared by coprecipitation method were the most selective to hydrogen production with CP10 giving the highest H<sub>2</sub> selectivity of 91 mol%, followed by CP15, 90 mol%. CP25 gave the lowest selectivity of 87 mol%. The catalysts prepared by the precipitation method gave a trend similar to that for the coprecipitation method. PT10 gave the highest selectivity of 87 mol% followed by PT15 and PT20 with equal selectivity

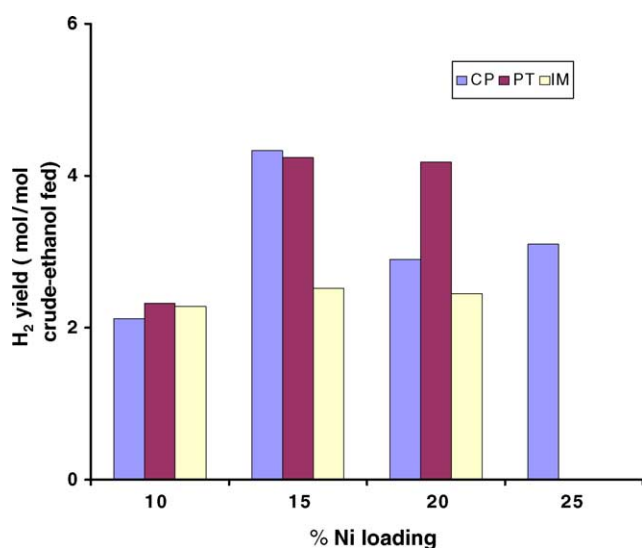


Fig. 11. Variation of hydrogen yield with Ni loading at  $T = 400\text{ }^{\circ}\text{C}$ , reduction temperature =  $600\text{ }^{\circ}\text{C}$ , calcination temperature =  $600\text{ }^{\circ}\text{C}$  and WHSV =  $1.68\text{ h}^{-1}$ .

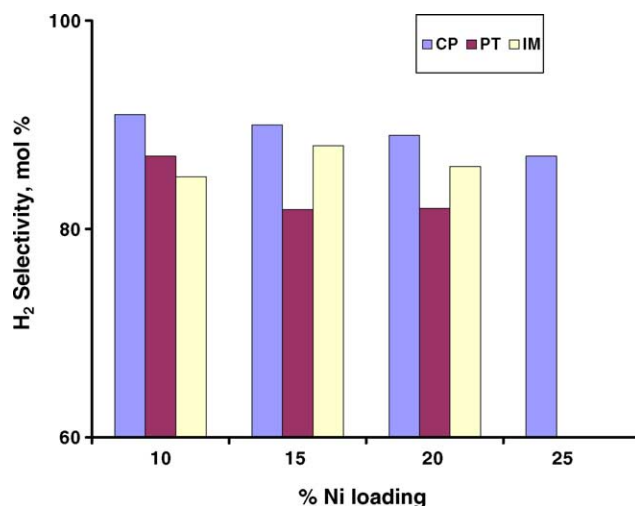


Fig. 12. Variation of hydrogen selectivity as a function of Ni loading at  $T = 400\text{ }^{\circ}\text{C}$ , reduction temperature =  $600\text{ }^{\circ}\text{C}$ , calcination temperature =  $600\text{ }^{\circ}\text{C}$  and WHSV =  $1.68\text{ h}^{-1}$ .

of 82 mol%. In contrast, catalyst prepared by the impregnation method showed a somewhat different trend, in which IM10 gave the lowest selectivity of 85 mol%. The selectivity reached a maximum of 88 mol% for IM15 and reduced to 86 mol% as the Ni loading increased to 20% in IM20.

### 3.2.5. Gas product distribution

Information on product distribution for all the catalysts is given in Table 6. The table shows that H<sub>2</sub> selectivity is generally affected by methanation and CO formation. For catalysts prepared by coprecipitation, the high H<sub>2</sub> selectivity obtained on CP10 and CP15 could be attributed to low methanation as well as low CO formation, which resulted in enhanced H<sub>2</sub> production. However, as Ni loading increased beyond 15%, the catalysts were more selective to CO formation at the expense of H<sub>2</sub> selectivity. On the other hand, low methanation was responsible for high H<sub>2</sub> selectivity obtained on PT10 as compared to PT15 and PT20. In the impregnation catalysts, however, low H<sub>2</sub> selectivity was obtained on IM10 and IM20, and was attributed to high CO formation as compared to what was obtained in IM15, which had the highest selectivity in this series.

Table 6  
Gas product distribution

	H <sub>2</sub>	CO <sub>2</sub>	CH <sub>4</sub>	CO	Conversion (X) (mol%)	S <sub>H<sub>2</sub></sub>
CP10	72.0	17.7	6.1	4.2	32.0	91.0
CP15	74.6	18.0	2.8	4.6	79.0	90.0
CP20	72.7	15.0	7.5	4.7	54.0	89.6
CP25	71.5	18.0	4.8	5.6	59.0	87.0
PT10	70.7	13.5	8.8	7.0	44.0	87.0
PT15	70.5	12.2	11.3	6.0	85.0	82.0
PT20	70.0	11.7	12.9	5.4	83.0	82.0
IM10	68.9	11.3	4.9	14.9	44.0	85.0
IM15	72.3	10.9	7.7	9.1	47.0	88.0
IM20	70.1	7.1	6.8	16.0	47.0	86.0

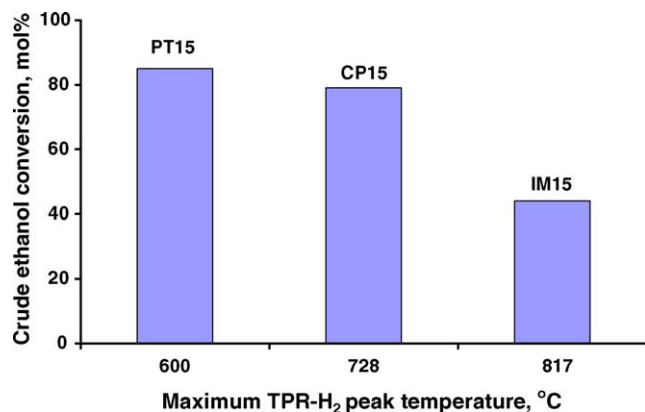


Fig. 13. Effects of reducibility on crude ethanol conversion on various catalysts.

In order to evaluate circumstances that led to a better performance of the PT and CP catalysts over the IM catalysts, we attempted to correlate the catalyst synthesis method to catalyst characteristics and to performance. Two catalyst characteristics, resulting from the three synthesis methods that exhibited a definite correlation with catalyst performance (in terms of crude ethanol conversion) were catalyst reducibility and crystallite size of Ni species.

### 3.2.6. Effect of catalyst reducibility on crude ethanol conversion

Earlier, we showed in Table 5 that the three synthesis methods had a strong effect on catalyst reducibility. Here we are evaluating whether and to what extent these differences in reducibility affected catalyst performance measured in terms of crude ethanol conversion. Reducibility was measured in terms of the minimum temperature required for complete reduction of the catalysts as provided by TPR-H<sub>2</sub> results (Fig. 5 and Table 5). Fig. 13 shows the typical effect of the reducibility of catalyst on conversion. PT15 was the most reducible catalyst because the dominant NiO species were completely reduced at 600 °C thereby making a larger amount of the active metal available for the reforming reaction. In contrast, the presence of NiAl<sub>2</sub>O<sub>4</sub> formed as a result of a strong metal–support interaction (see Eq. (2)) in both CP15 and IM15 made them less reducible as compared to PT15. The consequence is that a larger fraction of the Ni species were very tightly bound to the support, and therefore, not reduced at the reduction temperature used. Consequently, a small fraction of reduced active Ni metal species was available for the reforming reaction in both the CP and IM catalysts. Thus, while PT15 gave a crude ethanol conversion of 85% at the operating reduction temperature of 600 °C, CP15 and IM15 gave crude ethanol conversion of 79 and 46.7 mol%, respectively. Based on the latter two results, it would appear that the low crude ethanol conversion of 46.7 mol% for IM15 may not be solely due to reducibility factors as this alone should not produce such a drastic change.

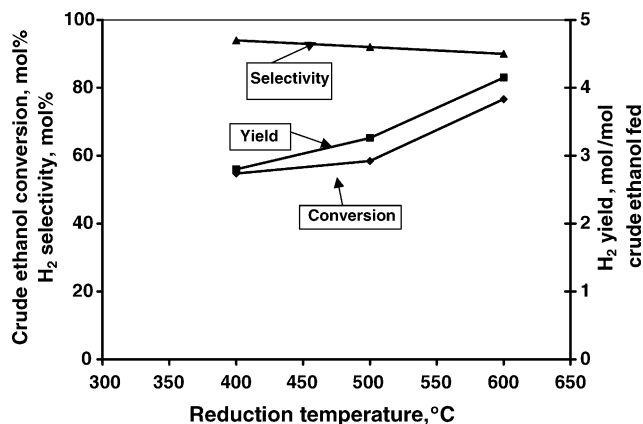


Fig. 14. Crude ethanol conversion, H<sub>2</sub> selectivity and H<sub>2</sub> yield as functions of reduction temperature for CP15 at  $T = 600$  °C, calcination temperature = 600 °C and WHSV = 1.68 h<sup>-1</sup>.

### 3.2.7. Effect of reduction temperature on crude ethanol conversion and hydrogen yield

In order to further probe the effect of reducibility on catalyst performance, experiments were also performed to determine the effect of changing the reduction temperature. All the experiments were conducted on CP15 using a  $W/F_{\text{crude-ethanol}}$  ratio of 0.59 h (i.e. WHSV = 1.68 h<sup>-1</sup>). The results are shown in Fig. 14. Crude ethanol conversion increased from 55 to 77 mol% and the hydrogen yield also increased from 2.8 to 4.2 mol/mol crude ethanol fed as the reduction temperature was increased from 400 to 600 °C. This result could be attributed to the small amount of the active Ni sites made available for the reforming reaction by reduction at the lower reduction temperature as compared with the amount available at higher temperatures. This can be confirmed from the TPR-H<sub>2</sub> profiles for catalyst CP15 (Fig. 5) in which this catalyst was more or less completely reduced at 600 °C. The figure further shows that the amount of Ni metal generated at 600 °C was definitely larger than those at 500 and 400 °C.

### 3.2.8. Effects of crystallite sizes on crude ethanol conversion

Earlier, we had attributed the major differences in performance of the catalysts prepared by the three methods to factors other than reducibility alone. One of these other factors was the crystallite size of the NiO species. Also, we had demonstrated that synthesis methods also affected the crystallite sizes of the active Ni species as observed in the X-ray line broadening results (Table 4). The effect of the synthesis method and Ni loading on the crystallite sizes and their ultimate effect on crude ethanol conversion are illustrated in Figs. 15–17. Fig. 15 shows the activities of catalysts prepared by coprecipitation method as a function of crystallite sizes and Ni loading. It is observed that an increase in Ni loading from 10% to 15% produces only a slight difference in crystallite size of the catalyst, but a large increase in crude ethanol conversion from 32 to 79 mol%.

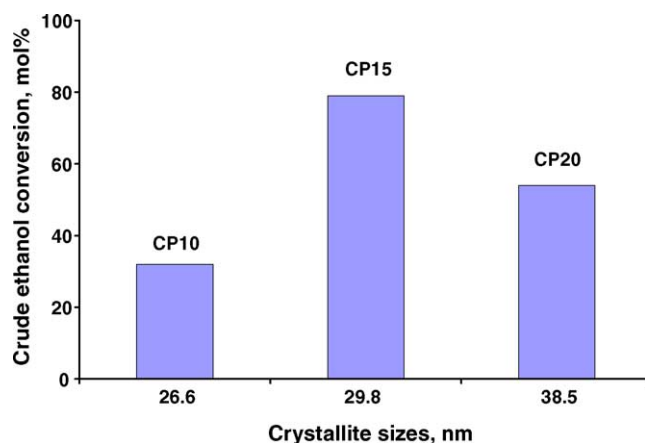


Fig. 15. Crude ethanol conversion as a function of crystallite size for catalysts prepared by the coprecipitation method.

This large increase is attributed to a larger amount of Ni being available because of the higher Ni loading of CP15 as compared to CP10. On the other hand, a further increase in Ni loading as in CP20 increased the crystallite size appreciably. This lowered the Ni dispersion on the catalyst such that the activity in CP20 dropped to 54 mol% even though its Ni loading was higher than CP15. In this case, the adverse effect of a larger crystallite size (lower Ni dispersion) outweighed the beneficial effect of Ni loading of CP20. Similar results were obtained when catalysts prepared by the precipitation method were used as shown in Fig. 16. The conversion dropped slightly when loading increased from 15% to 20%. The magnitude of change in this case is a reflection of the magnitudes of the detrimental effect of larger crystallite size as opposed to the beneficial effect of higher reducibility.

In the case of the catalysts prepared by the impregnation method, a completely different behavior was observed (Fig. 17). The crystallite size of IM10 was the smallest and there was a rapid increase in crystallite size as the Ni loading increased from 10% to 15% and a corresponding but slight increase in the activity of the catalysts with respect to crude

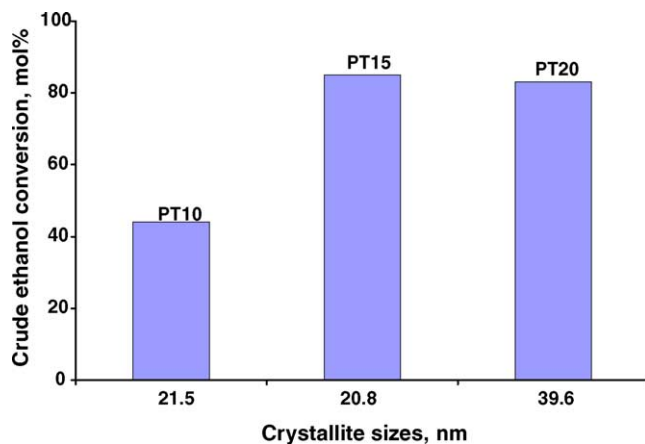


Fig. 16. Crude ethanol conversion as a function of crystallite size for catalysts prepared by the precipitation method.

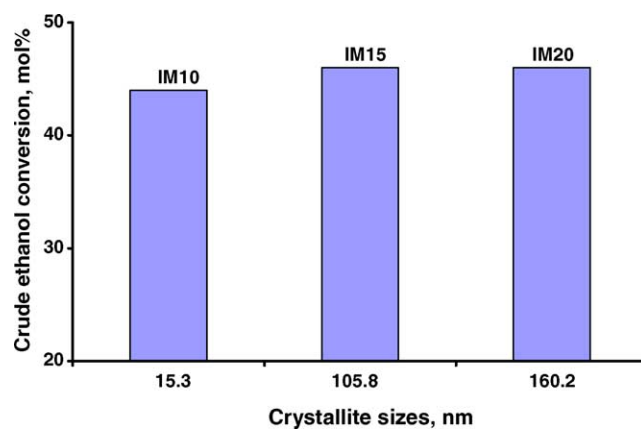


Fig. 17. Crude ethanol conversion as a function of crystallite size for catalysts prepared by the impregnation method.

ethanol conversion. For this preparation method, the beneficial effect of Ni loading of the catalysts appeared to have overcome the adverse effect of a larger crystallite size.

In all cases, it was observed that the crystallite size increased with Ni loading. Also, except for the IM series of catalysts, high Ni loading beyond 15% did not increase the activity with respect to crude ethanol conversion. This is in agreement with the results of Ming-Tseh and Chang [28] on supported Ni catalyst, in which the authors observed that at low nickel content the dispersion was higher than that at high nickel content and decreased gradually with loading. This was attributed to the fact that at low nickel content, the small nickel crystallites exhibit no agglomeration, while at high nickel content, there was the existence of agglomeration due to the presence of significant nickel density. These results on the effect of the crystallite size on catalyst performance explain the major difference between CP15 and IM15, which exhibited similar reducibility but widely different crude ethanol conversions. The results confirm that the major contributing factor in this case is the crystallite size of NiO species which is larger in IM15 (105.8 nm) as compared with CP15 (29.8 nm).

### 3.3. Effect of operating conditions

#### 3.3.1. Effect of temperature on crude ethanol conversion and hydrogen selectivity

Experiments were performed to study the effect of the reaction temperature on the overall crude ethanol conversion using CP15, as shown in Fig. 18. The reaction temperatures used were 320, 400, 420 and 520 °C for a fixed weight hourly space velocity of 1.68 h<sup>-1</sup>. As expected, crude ethanol conversion was lowest (64 mol%) at 320 °C and as the temperature was increased, the conversion increased and reached a maximum of 80.1 mol% at 520 °C. In contrast, the H<sub>2</sub> selectivity decreased with an increase in temperature, also as expected, due to the increased methanation activity as well as the formation of carbon monoxide on this catalyst at higher temperatures.

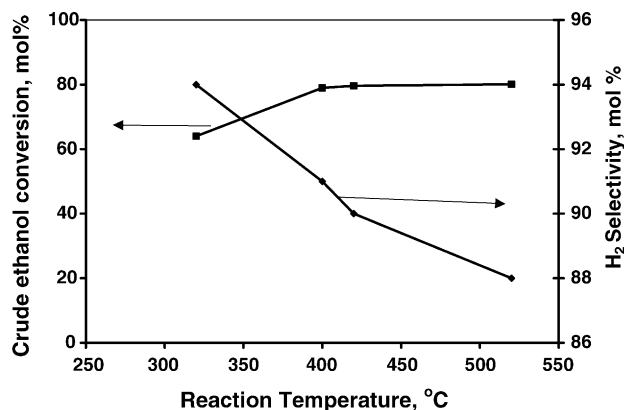


Fig. 18. Variation of crude ethanol conversion and hydrogen yield as a function of temperature for CP15 at reduction temperature = 600 °C, calcination temperature = 600 °C and WHSV = 1.68 h<sup>-1</sup>.

### 3.3.2. Effect of $W/F_{\text{crude-ethanol}}$ on crude ethanol conversion, hydrogen selectivity and yield

Experiments were also performed to study the effect of  $W/F_{\text{crude-ethanol}}$  ratio in the range 0.22–0.59 h (i.e. WHSV in the range 1.68–4.62 h<sup>-1</sup>) on crude ethanol conversion and hydrogen yield using CP15 at a reaction temperature of 420 °C. The results are given in Fig. 19, which shows that the conversion of crude ethanol increased from 35.6 mol% for  $W/F_{\text{crude-ethanol}}$  ratio of 0.22 h to 79.8 mol% for  $W/F_{\text{crude-ethanol}}$  ratio of 0.59 h. This behavior was expected as the reactant had a longer residence time for reaction inside the reactor. The effect of  $W/F_{\text{crude-ethanol}}$  ratio on hydrogen yield was similar to that for crude ethanol conversion as also shown in Fig. 19. The hydrogen yield increased from 1.95 to 4.33 (mol H<sub>2</sub>/mol crude ethanol feed) with an increase in  $W/F_{\text{crude-ethanol}}$  ratio from 0.22 to 0.59 h. The hydrogen selectivity also increased with  $W/F_{\text{crude-ethanol}}$  ratio. This result is contrary to what was expected. However, the result was attributed to the excess water that is present in crude ethanol.

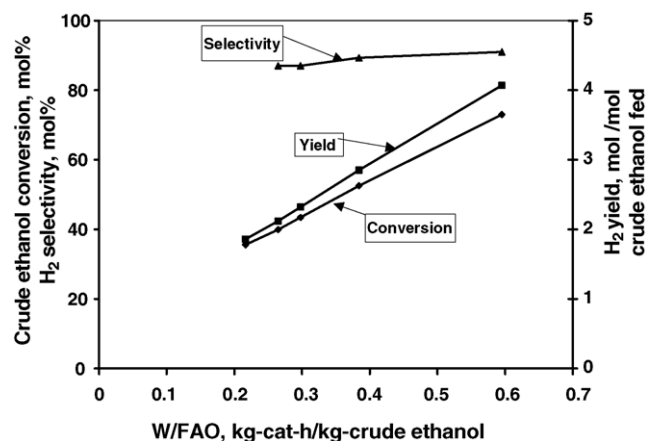


Fig. 19. Conversion of crude ethanol and H<sub>2</sub> selectivity as a function of  $W/F_{\text{crude-ethanol}}$  for CP15 at reduction temperature = 600 °C, calcination temperature = 600 °C and  $T = 420$  °C.

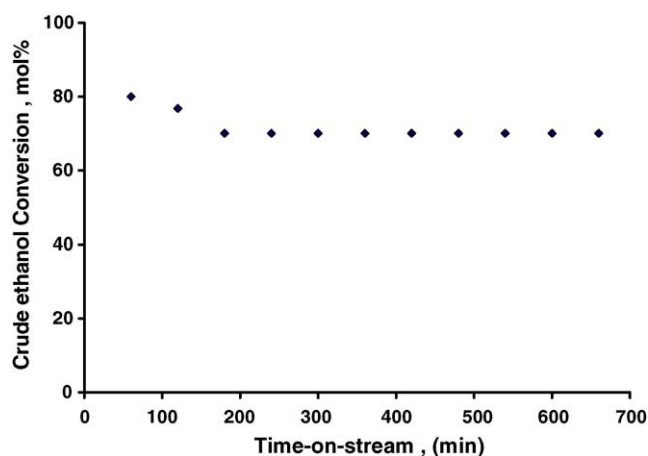


Fig. 20. Conversion of crude ethanol as a function of time-on-stream (min) for CP15 at  $T = 400$  °C, reduction temperature = 600 °C, calcination temperature = 600 °C and WHSV = 1.68 h<sup>-1</sup>.

### 3.4. Catalyst activity versus time-on-stream (TOS) studies

Catalyst activity was evaluated as a function of time-on-stream. This was conducted on the CP15 operating at a WHSV of 1.68 h<sup>-1</sup>, reduction temperature of 600 °C and a reaction temperature of 400 °C. Fig. 20 shows the crude ethanol conversion as a function of time-on-stream for 11 h of experimental run. The figure shows an initial wild activity, which dropped from 80 mol% to 70 mol% within the first 3 h of run and then stabilized for the remaining 8 h.

In order to determine whether the drop in activity was due to the conditioning of the catalyst in the reaction environment or due to coke formation, we decided to perform a temperature programmed oxidation (TPO) analysis of the spent sample obtained from the TOS studies. The results obtained for TPO carried out under oxidative atmosphere are given in Fig. 21. The figure shows a weight loss resulting from burning off of the coke deposited during the TOS run. This shows that coke deposition was the problem but appeared to have stabilized after 3 h. In the TPO profile itself, the initial step of weight reduction occurred

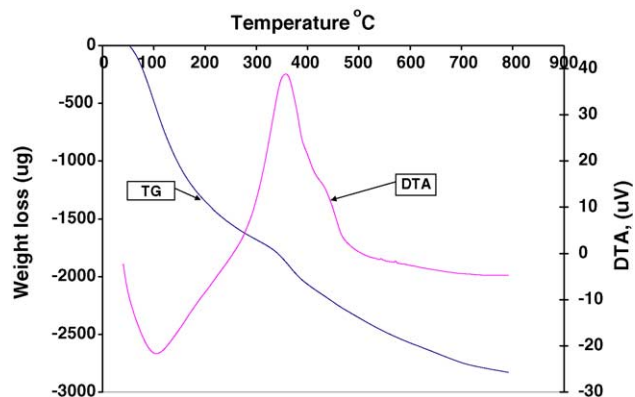


Fig. 21. The TPO profile of spent CP15 after 11 h time-on-stream.

over the temperature range of 100–200 °C. This was ascribed to the removal of easily oxidizable carbonaceous species, as reported by Das [16] and Jianjun et al. [22]. The oxidation of coke (carbon deposit) to CO and CO<sub>2</sub> occurred mainly at 360 °C. Further work is needed to investigate the catalyst stability for an economical length of time. This may lead to catalyst modification for the support and/or active metal.

### 3.5. Energy conversion efficiency—from crude ethanol to electrical energy

It is generally accepted that ethanol production is, at best, energy neutral. It thus becomes important to evaluate whether there is any benefit in terms of energy efficiency in further processing ethanol to produce hydrogen. Ethanol is used here solely for a niche application, which is the generation of mechanical or electrical energy. Thus, thermal efficiency alone is not the best way to measure efficiency in this case. Instead, what is of importance is the quantity of mechanical or electrical energy output from a unit quantity of ethanol. Thus, the efficiency of this process should be evaluated in terms of finding the best way to use ethanol for mechanical or electrical energy production. There are two methods to achieve this: (1) direct combustion of pure ethanol in an internal combustion engine to generate thermal energy and subsequent conversion of the thermal energy to produce mechanical energy, and (2) conversion of ethanol to hydrogen and subsequent use of hydrogen in a fuel cell to generate mechanical or electrical energy to power an engine. The following illustrates our calculations on the basis of 1 L of pure ethanol. As a fuel (in an internal combustion engine) in an automobile, only about 20% of the chemical energy stored in ethanol can be converted to useful mechanical work. On the other hand, if the same amount of ethanol is converted to hydrogen to run a fuel cell, about 60% of the stored chemical energy in hydrogen can be converted to electrical energy (Sorcha [5]).

#### 3.5.1. Case #1: ethanol as direct fuel for energy production

Chemical/heat energy available in pure ethanol ( $-\Delta H$ )

$$= 1000 \text{ mL} \times \frac{0.791 \text{ g}}{\text{mL}} \times \frac{27.76 \text{ kJ}}{\text{g}} = 21958.16 \text{ kJ}$$

With about 20% thermal energy to mechanical energy conversion efficiency, the useful mechanical work output (based on low heating value of ethanol (LHV)) =  $0.2 \times 21958.16 \text{ kJ} = 4391 \text{ kJ}$ .

#### 3.5.2. Case #2: crude ethanol as source of energy via the hydrogen fuel cell

Fermentation broth (from feedstock analysis) contains 12% (v/v) ethanol.

Amount of fermentation broth that will provide 1 L of ethanol =  $1/0.12 = 8.333 \text{ L}$  of feedstock.

Based on our results on reforming experiment using crude ethanol:

- $13.2 \times 10^{-3} \text{ L}$  (fermentation broth feedstock) produced 0.149 mol H<sub>2</sub>.
- 8.33 L (fermentation broth feedstock) will produce

$$\frac{8.33}{13.2 \times 10^{-3}} \times 0.149 = 94.028 \text{ mol of H}_2$$

Thus, the volume of H<sub>2</sub> produced = 94.028 mol  
 $\times 22.4 \text{ L/mol}$   
 = 2106.23 L

Heat energy available (based on LHV of H<sub>2</sub>) = 10.28 kJ/L<sub>H<sub>2</sub></sub>  
 $\times 2106.23 \text{ L}_{\text{H}_2} = 21652.04 \text{ kJ}$ .

With the assumption that the thermal energy carried by the reactor effluents can be used to heat the feed almost up to the reaction temperature, we only need to subtract the heat required for the reforming process from the heat available (i.e. less the heat required for reaction ( $-\Delta H_{\text{rxn}} = 129 \text{ kJ/mol}$ )).

Thus, the net heat =  $21652.04 \text{ kJ} - (129 \text{ kJ/mol} \times 15.13 \text{ mol}) = 19700.0 \text{ kJ}$ .

Assuming about 50% efficiency, the useful electrical work output =  $0.5 \times 19700 \text{ kJ} = 9850 \text{ kJ}$ . This is by far higher than the conversion efficiency obtained from a direct combustion of ethanol.

## 4. Conclusions

- The precipitation synthesis method resulted in the absence of NiAl<sub>2</sub>O<sub>3</sub> species in the catalysts whereas this species was a major component in catalysts prepared by the coprecipitation and impregnation synthesis methods.
- As a result of the type of species generated by the synthesis method, the PT catalysts were more reducible than the CP and IM catalysts.
- Catalysts prepared by precipitation generally exhibited lower crystallite sizes of NiO species than the corresponding catalysts prepared by coprecipitation. The catalysts prepared by impregnation had the largest crystallite sizes except IM10 which had the smallest crystallite size.
- A combination of small crystallite size and higher reducibility for PT catalysts resulted in higher crude ethanol conversions for the PT catalysts. These conversions were followed by those of the CP catalysts which had slightly bigger crystallite sizes but lower reducibility. The IM catalysts exhibited the lowest crude ethanol conversions because of larger crystallite sizes and lower reducibility.
- Catalysts with 15% Ni loading gave the best crude ethanol conversions for each method of synthesis with PT15

(catalyst with 15% Ni loading prepared by precipitation) giving the best overall crude ethanol conversion of 85 mol%. This was attributed to small crystallite size and high reducibility of PT15 as compared to CP15 and IM15.

- In terms of H<sub>2</sub> yield, CP15 gave the highest yield because the CP catalysts gave the highest H<sub>2</sub> selectivities as compared to corresponding catalysts prepared by precipitation and impregnation.
- Coking was observed at the onset of the reaction but stabilized after 180 min TOS.

## Acknowledgements

The financial support provided by the Canadian Foundation for Innovation and Hydrogen Thermochem Corporation (HTC), Regina, is gratefully acknowledged. The authors would also like to acknowledge the support of PoundMaker Agventure, Lanigan, Saskatchewan, Canada, for providing crude ethanol for the research.

## References

- [1] D. Cortright, R.R. Davda, J.A. Dumesic, *Lett. Nat.* 418 (2002) 964–967.
- [2] F. Haga, T. Nakajima, K. Yamashita, S. Mishima, *React. Kinet. Catal. Lett.* 63 (2) (1997) 253–259.
- [3] H.F. Creveling, Proceedings of the Annual Automotive Technology Development Contractors' Coordination Meeting, October 19–21, Society of Automotive Engineers, 1992, pp. 485–492.
- [4] D.S. Dunnison, J. Wilson, Proceedings of the AIAA 29th Intersoc. Energy Convers. Eng. Conference, Monterey, CA, 1994, pp. 1260–1263.
- [5] C. Sorcha, Faversham House Group Ltd., Internet publication, <http://www.edie.net/news/Archive/8065.cfm>, February 14, 2004.
- [6] J.H. Gary, G.E. Handwerk, *Petroleum Refining Technology and Economics*, third ed., Marcel Dekker Inc., New York, 1994.
- [7] V. Simanzhenkov, R.O. Idem, *Crude Oil Chemistry*, Marcel Dekker, New York, 2003.
- [8] L. Garcia, R. French, S. Czernik, E. Chornet, *Appl. Catal.* 201 (2000) 225–239.
- [9] S. Cavallaro, S. Freni, *Int. J. Hydrogen Energy* 21 (6) (1996) 465–469.
- [10] N.F. Athanasio, X.E. Verykios, *J. Catal.* 225 (4) (2004) 39–452.
- [11] N.F. Athanasio, D.I. Kondarides, *Catal. Today* 75 (2002) 145–155.
- [12] V. Klouz, V. Fierro, P. Denton, H. Katz, J.P. Lisse, S. Bouvot-mauduit, C. Mirodatos, *Power Sources* 105 (2002) 26–34.
- [13] L. Jordi, N. Homs, J. Sales, P. Ramirez de la Piscina, *J. Catal.* 209 (2002) 306–317.
- [14] S. Leclerc, R.F. Mann, B.A. Peppley, Evaluation of the catalytic ethanol-steam reforming process as a source of hydrogen-rich gas for fuel cells, Report prepared for CANMET Energy Technology Centre (CETC), 1998, ISBN 0-662-27335-4.
- [15] V.V. Galvita, G.L. Semin, V.D. Belyaev, V.A. Semikolenov, P. Tsia-karas, V.A. Sobyenin, *Appl. Catal. A: Gen.* 220 (2001) 123–127.
- [16] N. Das, M.Sc. Thesis, University of Saskatchewan, Saskatoon, Canada, 2003.
- [17] R. Idem, H.H. Ibrahim, P. Tontiwachwuthikul, M. Wilson, in: J. Gale, Y. Kaya (Eds.), *Proceedings of the 6th International Conference on Greenhouse Gas Control Technologies*, Kyoto, Japan, 2002, Pergamon, Oxford, UK, 2003, pp. 1825–1828.
- [18] W. Iwasaki, *Int. J. Hydrogen Energy* 28 (2003) 1325–1332.
- [19] C.A. Luengo, G. Ciampi, M.O. Cencig, C. Steckelberg, M.A. Larbode, *Int. J. Hydrogen Energy* 17 (9) (1992) 667–681.
- [20] J.T. Richardson, *Principles of Catalyst Development*, Plenum Press, New York, 1989.
- [21] R.O. Idem, Ph.D. Thesis, University of Saskatchewan, Saskatoon, Canada, 1995.
- [22] G. Jianjun, H. Lou, H. Zhao, D. Chai, X. Zheng, *Appl. Catal. A: Gen.* 273 (2004) 75–82.
- [23] B. Parathasarathi, M. Rajamathi, M.S. Hegde, P.V. Kamath, *Bull. Mater. Sci.* 23 (2) (2000) 141–145.
- [24] R.O. Idem, S.P.R. Katikaneni, R. Sethuraman, N.N. Bakhshi, *Energy Fuel* 141 (2000) 1072–1082.
- [25] E.L. Jae-Hee, J. Oh-shim, J. Kwang, *Appl. Catal. A: Gen.* 269 (2004) 1–6.
- [26] F. Marino, E. Cerrella, S. Duhalde, M. Jobbagy, M. Laborde, *Int. J. Hydrogen Energy* 23 (1998) 1095–1101.
- [27] J. Juan-Juan, M.C. Roman-Martinez, M.J. Illan-Gomez, *Appl. Catal. A: Gen.* 264 (2004) 169–174.
- [28] T. Ming-Tsch, F. Chang, *Appl. Catal. A: Gen.* 203 (2002) 15–22.